EUROPEAN TRANSACTIONS ON ELECTRICAL POWER
Euro. Trans. Electr. Power 2005; **15**:245–256
Published online in Wiley InterScience (www.interscience.wiley.com). DOI: 10.1002/etep.56

Design, modelling and test results of the AWS PM linear generator

H. Polinder[1,*,†] M. E. C. Damen[2] and F. Gardner[2]

[1]*Delft University of Technology, Electrical Engineering, Electrical Power Processing, Mekelweg 4, 2628 CD Delft, The Netherlands*
[2]*Teamwork Technology B.V., De Weel 20, 1736 KB Zijdewind, The Netherlands*

SUMMARY

The Archimedes Wave Swing (AWS) is a system that converts ocean wave energy into electrical energy. A pilot plant of this system has been built. This paper describes the design of the permanent-magnet (PM) linear synchronous generator applied in the AWS. Based on a magnetic circuit model, it is concluded that saturation does not play an important role. The correlation between measured and calculated generator parameters and no-load voltage is reasonable, which indicates that the generator is adequate. Copyright © 2005 John Wiley & Sons, Ltd.

KEY WORDS: Archimedes Wave Swing (AWS); wave energy; permanent-magnet linear generator

1. INTRODUCTION

There are various ways of converting ocean wave energy into electric energy, as shown in References [1–6]. The Archimedes Wave Swing (AWS) concept is unique because it is completely submerged. This is important, because it makes the system less vulnerable in storms; and it is not visible, so that public acceptance is not as much of a problem as it is, for example, with offshore wind farms.

The AWS basically is a cylindrical air-filled chamber as shown in Figure 1. The lid of this chamber, called the floater, can move in a vertical direction with respect to the bottom part, which is fixed to the sea-bottom. When a wave is above the AWS, the volume of the AWS is reduced by the high pressure of the water. When a trough is above the AWS, the volume increases because of the air pressure inside the AWS. From this linear motion, energy can be extracted.

By tuning the system frequency to the wave frequency, the stroke of the linear motion can be made much higher than the wave height. The system frequency can be changed by changing the air pressure and the volume inside the AWS.

It is possible to convert the linear motion to rotating motion and thus use a rotating generator. However, it appears to be extremely difficult to build a robust and maintenance-free gear; therefore, a linear generator is used.

The generator terminals are connected to a 6 km long cable, which brings the power to the shore. An inverter on the shore is used for the utility grid connection.

*Correspondence to: H. Polinder, Delft University of Technology, Electrical Engineering, Electrical Power Processing, Mekelweg 4, 2628 CD Delft, The Netherlands.
†E-mail: H.Polinder@EWI.TuDelft.nl

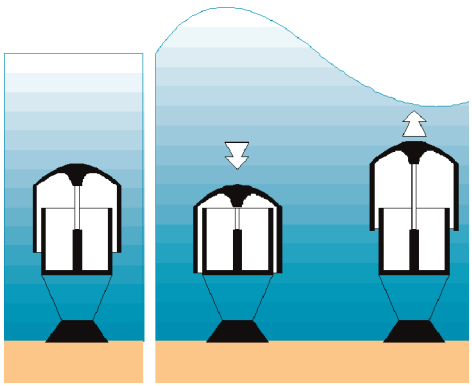

Figure 1. Operating principle of the AWS.

Calculations and tests on the hydrodynamic performance have been reported in References [7,8]. In References, [9,10], the results have been used for energy yield calculations. An early description of the generator system has been reported in Reference [9]. Since then, the design has been changed and a pilot plant has been built.

The objective of this paper is to describe the generator design. The paper first describes the pilot plant; then the generator design and performance are discussed. Subsequently, a generator model including saturation is derived and the results of some generator tests are presented. The paper ends with some conclusions.

2. PILOT PLANT DESCRIPTION

A pilot plant of the AWS has been built on the coast of Portugal. The AWS was submerged in May 2004. It has been converting wave energy into electrical energy since October 2004. Further

Figure 2. The AWS pilot plant before submersion.

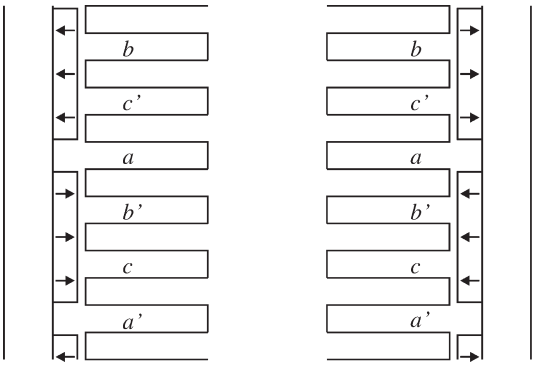

Figure 3. Section of a generator part.

analysis of the measurements will take some more time. Figure 2 shows the pilot plant. The centre part contains the floater that moves up and down. The floater diameter is 9 m and the stroke is 7 m (rated) or 9 m (maximum). The main objectives of this pilot plant are to prove the survivability of the system, and to prove the system works. Scale models have been successfully tested [8], but the complete system has not yet been tested.

It is nearly impossible to make the generator large enough to take all possible forces generated by waves. Therefore, the AWS also has water dampers that can take very high forces. This implies that the generator is not dimensioned to take the maximum force. It can be designed as a compromise between energy yield and cost.

The linear generator that converts the mechanical energy into electrical energy is a permanent-magnet (PM) generator because:

- it has a rather high force density,
- it has a rather high efficiency at low speeds, and
- there is no electrical contact between the moving part (the translator) and the stator, which is important because such an electrical contact suffers from wear.

To balance the attractive forces between stator and translator, the generator is double sided, as shown in Figure 3. Figure 4 shows a translator segment with magnets on back iron. The magnets are skewed to reduce cogging. Figure 5 shows a stator segment with its winding.

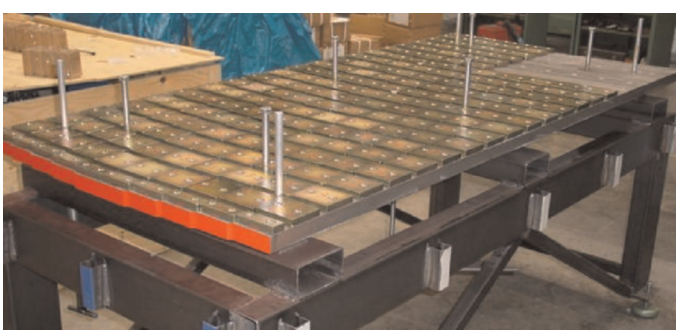

Figure 4. Translator segment with magnets in production.

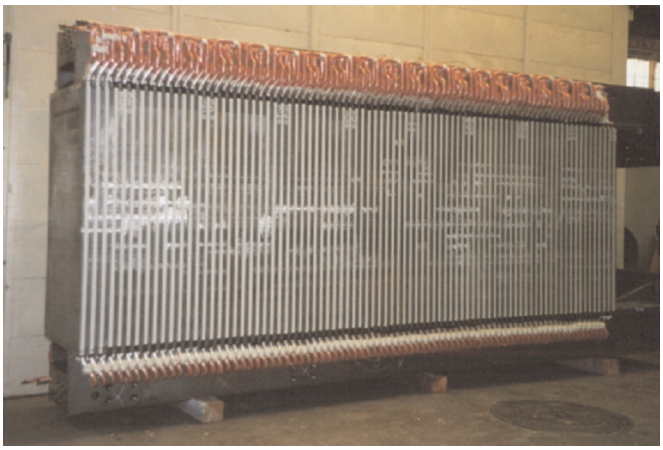

Figure 5. A stator segment with coils.

3. GENERATOR DESIGN

3.1. Generator use

It is assumed that a back-to-back voltage source inverter is used. This choice makes it possible to vary the angle between no-load voltage and current.

Using current in phase with no-load voltage results in the lowest copper losses. However, the flux density level is increased, which may result in saturation, and the converter has to be significantly over-dimensioned because of the low converter power factor.

Using current in phase with terminal voltage results in the smallest converter but limits the power that can be taken from the generator significantly.

Therefore, the phase of the current I_s is in the middle between the phase of the no-load-voltage E_p and the terminal voltage as indicated in the phasor diagram of Figure 6.

3.2. Pole-pitch layout and demagnetization

A cross-section of two generator pole-pitches is depicted in Figure 3. A three-phase machine is chosen because most available inverters have three phases.

The number of slots per pole is chosen as three. Increasing the number of slots whilst keeping the pole-pitch constant would result in a much smaller slot area available for the copper windings, or in

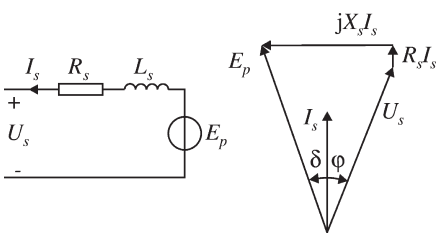

Figure 6. Equivalent circuit of the PM linear synchronous machine and the phasor diagram.

extremely long and thin stator teeth. Increasing the number of slots and increasing the pole-pitch would result in a much larger main inductance, which increases the risk of magnet demagnetization. In the chosen pole-pitch layout, the leakage inductance of the stator coils is larger than the main inductance, so that the magnets are not demagnetized in the case of a short circuit [11].

3.3. Generator parameters

The machine parameters are calculated in conventional ways. Slot, air-gap and end-winding leakage inductances are calculated as in Reference [12]. The effective air gap of the machine is calculated as

$$\begin{aligned} g_{\text{eff}} &= g_1 k_{\text{C}} \\ g_1 &= g + \frac{l_{\text{m}}}{\mu_{\text{rm}}} \\ k_{\text{C}} &= \frac{b_{\text{s}} + b_{\text{t}}}{b_{\text{s}} + b_{\text{t}} - \gamma g_1} \\ \gamma &= \frac{4}{\pi}\left(\frac{b_{\text{s}}}{2g_1}\arctan\frac{b_{\text{s}}}{2g_1} - \log\sqrt{1+\left(\frac{b_{\text{s}}}{2g_1}\right)^2}\right) \end{aligned} \tag{1}$$

where k_{C} is the Carter factor [12], g is the mechanical air gap, l_{m} is the magnet length in the magnetization direction, μ_{rm} is the recoil permeability of the magnets, b_{t} is the tooth width, and b_{s} is the slot width.

The main inductance is calculated as

$$L_{\text{sm}} = \frac{6\mu_0 l_{\text{s}} \tau_{\text{p}} (k_{\text{w}} N_{\text{s}})^2}{p\pi^2 g_{\text{eff}}} \tag{2}$$

where μ_0 is the magnetic permeability in vacuum, l_{s} is the machine stack length perpendicular to the plane of the drawing in Figure 3, τ_{p} is the pole pitch, N_{s} is the number of turns of the winding, k_{w} is the winding factor, and p is the number of pole pairs.

The fundamental space harmonic of the magnetic flux density in the air gap due to the magnets is given by

$$\hat{\boldsymbol{B}}_{\text{gm}} = \frac{l_{\text{m}}}{\mu_{\text{rm}} g_{\text{eff}}} B_{\text{rm}} \frac{4}{\pi} \sin\left(\frac{\pi b_{\text{p}}}{2\tau_{\text{p}}}\right) \tag{3}$$

where B_{rm} is the remanent flux density of the magnets, and b_{p} is the magnet pole width.

The no-load voltage induced by this flux density in a stator winding is

$$E_{\text{p}} = \sqrt{2} l_{\text{s}} N_{\text{s}} k_{\text{w}} v \hat{\boldsymbol{B}}_{\text{gm}} \tag{4}$$

where v is the floater velocity.

The stator phase resistance is calculated from the machine dimensions, the number of turns in a slot and the cross-section of a slot:

$$R_{\text{s}} = \rho_{\text{Cu}} \frac{l_{\text{Cus}}}{A_{\text{Cus}}} = \rho_{\text{Cu}} \frac{2N_{\text{s}}^2 (l_{\text{s}} + 2\tau_{\text{p}})}{p h_{\text{s}} b_{\text{s}} k_{\text{sfil}}} \tag{5}$$

where ρ_{Cu} is the resistivity of copper, h_{s} is the slot width, and k_{sfil} is the copper fill factor of the slots.

3.4. Generator losses

The generator has to function as a damper, the damping of which depends on the wave period and the wave amplitude [9]. Therefore, the generator force has to be proportional to the floater velocity. From the generator force, the current can be calculated using the phasor diagram of Figure 6.

The stator copper losses can then be calculated with

$$P_{\mathrm{Cus}} = 3R_{\mathrm{s}}I_{\mathrm{s}}^2 \tag{6}$$

The stator iron losses are calculated as

$$P_{\mathrm{Fes}} = 2P_{\mathrm{Fe0}}\left(m_{\mathrm{Fest}}\left(\frac{b_{\mathrm{s}}+b_{\mathrm{t}}}{b_{\mathrm{t}}}\right)^2 + m_{\mathrm{Fesy}}\left(\frac{\tau_{\mathrm{p}}}{\pi h_{\mathrm{sy}}}\right)^2\right)\frac{f_{\mathrm{e}}}{f_0}\left(\frac{\hat{B}_{\mathrm{gm}}}{B_0}\right)^2 \tag{7}$$

where P_{Fe0} is the iron loss per unit mass at a frequency f_0 and flux density B_0 provided by the material manufacturer, m_{Fest} is the mass of the stator teeth, m_{Fesy} is the mass of the stator yoke, f_{e} is the electrical generator frequency, and h_{sy} is the stator yoke height.

In this expression, the iron losses are assumed to be proportional to the frequency. Mostly, iron losses are calculated as the sum of the hysteresis losses, which are proportional to the frequency, and the eddy-current losses, which are proportional to the frequency squared. Because of the low frequencies, assuming the losses to be proportional to the frequency means the iron losses are overestimated. The factor 2 is included because punching deteriorates the material properties and because the flux densities do not change sinusoidally, which increases the iron losses [13].

3.5. Generator surface optimization

Using the pole-pitch layout discussed in Section 3.2, the generator surface has to be determined. The generator surface is defined as the stack length l_{s} multiplied by the length in the motion direction.

When the generator surface is increased, the generator efficiency increases, but it also becomes more expensive. The generator surface is determined by an optimization program. We used the criterion that an extra investment in active generator material has to be paid back by an increased energy yield within ten years, as calculated in References [9,10]. The stator length and the translator length are optimized independently.

The resulting translator length is a few metres more than the resulting stator length. This means that during a large part of the floater stroke, the overlap between the stator and the translator is partial. This could be expected because, near the stroke end, the required force is rather small.

A liquid cooling system removes the heat from the machine. It is important to realize that it is not necessary to design this cooling system for peak force. This peak force lasts only a part of a period and, even in the heaviest sea-state, only a part of the waves is so heavy that this peak force is necessary. Therefore, the machine cooling is designed to remove the average dissipation during the heaviest sea-state.

3.6. Generator performance

Figure 7 illustrates the machine performance during half a wave period for a rather heavy wave. The wave force, the floater position, and the floater speed are sinusoidal functions of time.

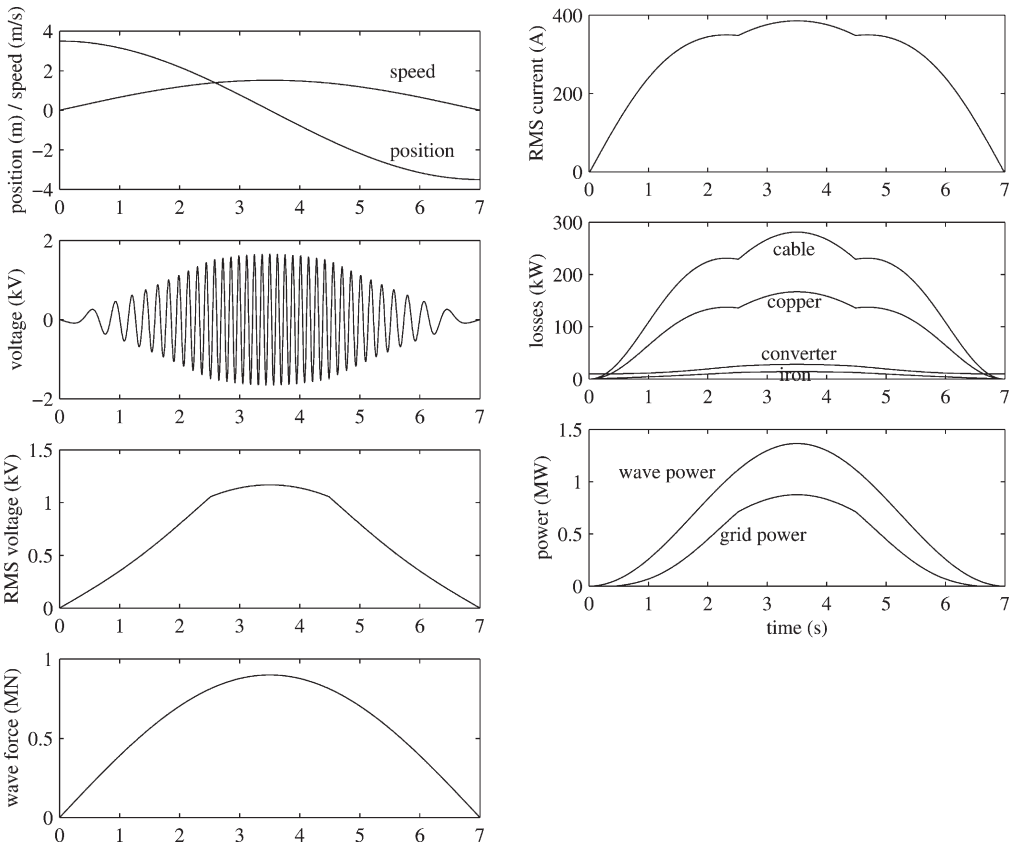

Figure 7. Position, speed, no-load phase voltage, RMS no-load phase voltage, generated force, RMS current, losses and powers as functions of time during half a wave period.

The RMS value of the voltage is not exactly proportional to the speed because the overlap between stator and translator changes. The required force is proportional to the speed and depends on the wave amplitude and the wave period. To make this force, a current is injected in the stator. Here, it is assumed that this current is in phase with the no-load voltage. The RMS value of the current does not vary sinusoidally because the overlap between the stator and the translator changes. When the overlap reduces, the current has to increase to obtain the required force.

The losses in the converter are assumed to be 2.5% of the rated power at full load, 0.5% of the rated power in no-load and 2% proportional to the actual power delivered by the converter.

As can be concluded from Figure 7, a substantial part of the energy taken from the waves is dissipated in the generator and the cable. Fortunately, the efficiency in part load, where the AWS usually operates, is better. Figure 8 depicts the generator efficiency averaged over a wave period.

The grid power varies as a squared sinus. The annual energy supplied to the utility grid is calculated as 1.94 GWh. This means that the average power supplied to the grid is 221 kW. For an installed peak power of 2 MW, this is rather low.

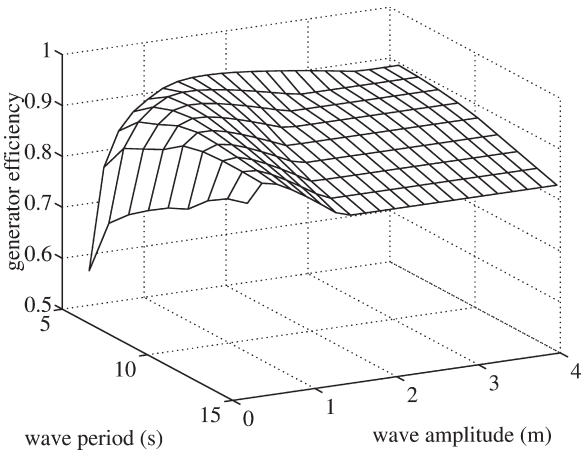

Figure 8. Generator efficiency averaged over a wave period as a function of wave amplitude and wave period.

4. MODELLING SATURATION

At high current levels, the generator iron saturates. Saturation can be modelled using finite element methods (FEM). However, a first estimate of the consequences of saturation can be obtained by using a magnetic circuit model with variable reluctances for the saturating parts [14–16]. In this model, the magnetic fluxes in the teeth are the most important, because these fluxes link with the stator coils which are used in the force calculation.

Figure 3 gives a cross-section of two generator pole-pitches. In order to obtain a simple model, end effects are neglected. Because the stator yoke and the translator back-iron are thick, their reluctances are neglected, so that only the stator teeth saturate. By making the stator tooth reluctances a function of the flux density, saturation is modelled. The resulting model is given in Figure 9. Because end effects are neglected, the left and the right side of this model can be connected. By using the symmetry within this network, it can be solved using only half of it.

A general expression for the value of a reluctance is

$$R_{\mathrm{m}} = \frac{l_{\mathrm{c}}}{A_{\mathrm{c}}}\frac{H}{B} \tag{8}$$

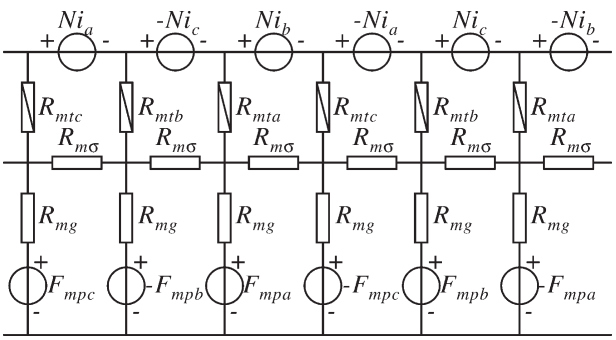

Figure 9. Magnetic circuit model of two pole-pitches of the generator.

where H is the magnetic field intensity in the circuit, B is the magnetic flux density in the circuit, l_c is the length of the magnetic circuit, and A_c is the cross-section of the magnetic circuit.

With this, the air gap reluctance R_{mg} (the reluctance between a tooth and the back-iron) can be expressed as

$$R_{mg} = \frac{(g + l_m/\mu_{rm})k_C}{\mu_0(b_s + b_t)l_s} \tag{9}$$

The slot leakage reluctance $R_{m\sigma}$ is calculated as

$$R_{m\sigma} = 0.9\frac{2b_s}{\mu_0 h_s l_s} \tag{10}$$

Half the slot height h_s is used in the circuit surface because the leakage flux density in the slot increases from zero close to the yoke to maximum close to the air gap. The factor 0.9 is there to consider air-gap leakage.

The starting point for the determination of the tooth reluctance is the *BH*-curve of the magnetic material. This *BH*-curve is approximated by

$$H = 400B + 7B^{13} \tag{11}$$

Using this in Equation (8), the tooth reluctance R_{mt} can be calculated as

$$R_{mt} = \frac{2h_s}{3b_t l_s}(400 + 7B_t^{12}) \tag{12}$$

In this equation, the circuit surface is the tooth cross-section, and the length is taken as two-thirds of the tooth height. Two-thirds of the tooth height is taken because leakage flux enters the tooth over the whole height, so that the part close to the air gap does not saturate or saturates later.

When a tooth pitch is completely covered by a magnet, the magnetomotive force of this magnet causing a flux in this tooth is the magnet length multiplied by the coercive force: $l_m H_c$. When the tooth pitch is not completely covered by a magnet, the magnetomotive force causing a flux in this tooth is smaller. In this way, the magnetomotive force of a magnet is a function of the position x. This function is approximated by

$$F_m = l_m H_c\left(1.16\sin\left(\frac{\pi}{\tau_p}x\right) + 0.16\sin\left(3\frac{\pi}{\tau_p}x\right)\right) \tag{13}$$

With this model, the fluxes can be solved via a numerical iteration. Forces can be calculated using co-energy [17], as worked out in Reference [15,16].

Figure 10 depicts the force as a function of the position and the current. When the machine saturates, the force becomes a function of the position, which is periodic with the tooth pitch. It can be concluded that for currents up to 400 A, saturation hardly plays a role.

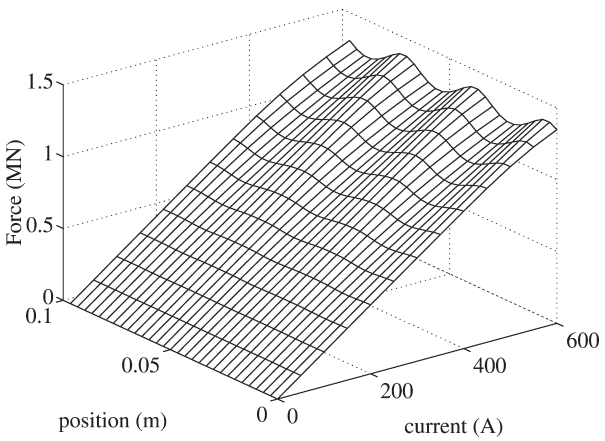

Figure 10. Generated force as a function of position and current.

5. MEASURED PARAMETERS AND NO-LOAD VOLTAGE

When the translator segments with the magnets were hoisted into the AWS, they moved along the stator, and the voltage induced in the stator phases was measured. Figure 11 gives the no-load voltage of a part of the generator at very low and not exactly constant speed (a few centimetres per second). The no-load voltage decreases while the frequency remains more or less constant because the overlap between the stator and the translator decreases.

By integrating the no-load voltage, the flux linkage was obtained. Figure 11 also depicts this flux linkage during an interval where the stator was completely overlapping the translator with the magnets. This flux linkage appears to be sinusoidal.

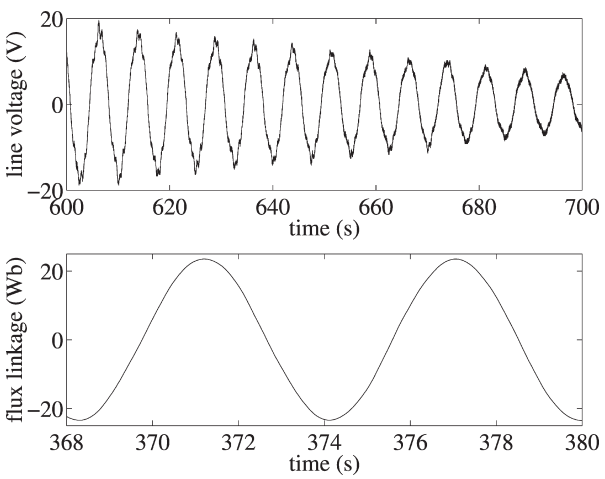

Figure 11. Measured no-load line voltage and flux linkage of a part of the generator.

Table I. Comparison of measurements and calculations.

	Calculated	Measured
Flux linkage, λ_{pp}	46 Wb	47 Wb
Leakage inductance, L	28 mH	31 mH
Resistance, R	0.27 Ω	0.29 Ω

As can be seen from Table I, the value of the flux linkage correlates well with the calculated flux linkage. The resistance and inductance of the generator were determined by measuring the current response to a step voltage. Also, here the correlation between measurement and calculation is reasonable.

6. CONCLUSIONS

A permanent-magnet linear synchronous generator for application in the AWS has been designed and built. Based on a magnetic circuit analysis, it is concluded that saturation does not play an important role in this generator. The correlation between measured and calculated quantities is reasonable, which indicates that the generator design is working appropriately.

REFERENCES

1. Meyer NI, Nielsen K. The Danish wave energy programme second year status. *Proceedings of the Fourth Wave Energy Conference*, Aalborg, 2000, pp. 10–18.
2. Thorpe TW. The wave energy programme in the UK and the European wave energy network. *Proceedings of the Fourth Wave Energy Conference*, Aalborg, 2000, pp. 19–27.
3. Thorpe TW. *A review of wave energy*. ETSU report, R-72, 1992.
4. Mueller MA. Electrical generators for direct drive wave energy converters. *IEE Proceedings—Generation, Transmission and Distribution* 2002; **149**:446–456.
5. Mueller MA, Baker NJ, Spooner E. Electrical aspects of direct drive wave energy converters. *Proceedings of the Fourth Wave Energy Conference*, Aalborg, December 2000.
6. Narayanan SSY, Murthy BK, Rao GS. Dynamic analysis of a grid-connected induction generator driven by a wave-energy turbine through hunting networks. *IEEE Transactions on Energy Conversion* 1999; **14**:115–121.
7. Sarmento AJNA, Luíd AM, Lopes DBS. Frequency-domain analysis of the AWS device. *European Wave Energy Conference*, Patras, 1998.
8. Rademakers LWMM, Van Schie RG, Schuitema R, Vriesema B, Gardner F. Physical model testing for characterising the AWS. *European Wave Energy Conference*, Patras, 1998.
9. Polinder H, Gardner F, Vriesema B. Linear PM generator for wave energy conversion in the AWS. *Proceedings of the Eighth International Conference on Electrical Machines*, Helsinki, 2000, pp. 309–313.
10. Polinder H, Damen M, Gardner F. Linear PM generator system for wave energy conversion in the AWS. *IEEE Transactions on Energy Conversion*, 2004; **19**:583–589.
11. Sebastian T, Slemon GR. Transient torque and short-circuit capabilities of variable speed permanent magnet motors. *IEEE Transactions on Magnetics* 1987; **23**:3619–3621.
12. Richter R. *Elektrische Maschinen, Erster Band* (3rd edn). Birkhäuser: Basel, 1967.
13. Slemon GR, Liu X. Core losses in permanent-magnet motors. *IEEE Transactions on Magnetics* 1990; **26**:1653–1655.
14. Ostovic V, Miller JM, Grag VK, Schultz RD, Swales SH. A magnetic-equivalent-circuit-based performance computation of a Lundell alternator. *IEEE Transactions on Industry Applications* 1999; **35**:825–830.
15. Polinder H, Slootweg JG, Hoeijmakers MJ, Compter JC. Modelling a linear PM motor including magnetic saturation. *Proceedings of the International Conference on Power Electronics, Machines and Drives*, Bath, 2002, pp. 632–637.
16. Polinder H, Slootweg JG, Hoeijmakers MJ, Compter JC. Modelling a linear PM machine including magnetic saturation and end effects: maximum force to current ratio. *IEEE Transactions on Industry Applications* 2003; **39**:1681–1688.
17. Fitzgerald AE, Kingsley C, Umans SD. *Electric Machinery* (6th edn). McGraw-Hill: London, 2003.

AUTHOR'S BIOGRAPHIES

Henk Polinder was born in Nunspeet, the Netherlands, in 1968. He received the M.Sc. and Ph.D. degrees from Delft University of Technology in 1992 and 1998, respectively. From 1996 to 2003, he was an assistant professor and since 2003 he has been an associate professor in the Electrical Power Processing group of Delft University of Technology. He is mainly interested in design aspects of electrical machines for renewable energy (wind and waves) and mechatronic applications.

Michiel Damen was born in The Hague, the Netherlands, in 1976. He received his B.Sc. degree from the Technical Highschool Rijswijk in 1998 and the M.Sc. degree from Delft University of Technology in 2003. Currently, he is part-time employed by AWS and Technical Highschool Rijswijk. Electrical power aspects of renewable energy sources are his main interest.

Fred Gardner was born in Brisbane, Australia, in 1956, and immigrated to the Netherlands in 1963. He is educated as engineer in mechanics and electrics and teaching. Since 1993, he is director engineering of Teamwork Technology BV, where he is responsible for concept engineering and product development of products such as the Archimedes Wave Swing. His special interest is the management of the innovation process.